Multiple Access Interference in Time Hopping Ultra-Wideband Radio

Norman C. Beaulieu and Bo Hu

Dept. of Electrical and Computer Eng., University of Alberta, Edmonton, Alberta, Canada

ABSTRACT

A method is proposed for precisely analyzing the effects of the multiple access interference in the time-hopping ultra-wideband communication systems on the average symbol error rates. An exact analysis is derived for calculating the bit error probability of ultra-wideband systems operating in multiple access interference. The analytical expressions are validated by simulation and used to assess the accuracy of the Gaussian approximation, a widely adopted method for evaluating bit error rate performance. The Gaussian approximation is shown to be inaccurate for predicting bit error rates for medium and large signal-to-noise power ratio values. The different time-hopping modulation schemes are accurately assessed in terms of their sensitivities to the system parameters and the bit error rate.

Keywords: Error rate analysis, multiple access, time-hopping, ultra-wideband

1. INTRODUCTION

The newest topic in wireless research is ultra-wide bandwidth (UWB) wireless systems. The Federal Communications Commission (FCC) in the United States has only recently approved the operation of UWB systems; other countries have not yet approved UWB system operation, but their plannings for approval are in advanced stages of progress. The operation of UWB systems and devices is unlicensed operation. However, the use of UWB systems and devices is regulated in the sense that the UWB wireless signals must meet specified frequency spectrum emission power levels. In UWB systems, the wireless signal is intentionally spread over an extremely wide bandwidth, typically several gigahertz. The FCC defines UWB systems as radio systems having signal waveforms with fractional bandwidths greater than 25%, which is given by

$$\text{Fractional Bandwidth} = \frac{f_H - f_L}{2(f_H + f_L)} > 25\%$$

where f_H is the upper 10 dB down point and f_L is the lower 10 dB down point of the power spectrum of the transmitted signals. The relationship between the power spectrums of narrowband and UWB systems is shown in Fig. 1. Note that UWB system design is contrary to the usual practice of attempting to make the wireless signal occupy as little bandwidth as possible.

Also contrary to usual radio system practice, UWB radio does not use a radio frequency carrier. Rather, extremely short duration electrical pulses (or impulses) are specially shaped to achieve the desired spectral emission characteristics without putting the electrical pulses on a radio frequency carrier. The great bandwidth and the property that UWB works in a carrierless manner distinguish UWB systems from conventional narrowband and carrier-based systems. The UWB signal will have a very small power spectral density per unit bandwidth (Hertz) because the signal energy is being spread over such a large bandwidth. Therefore, the UWB signal will appear basically as low power "noise" to other UWB users, and to other radio devices and systems. Thus, UWB can be used as a multiple access technique by several users, or as "tolerable" co-existing interference with other radio devices or systems. UWB signals can share frequency spectrum with narrowband and other UWB systems with proper design. Considering the proliferation of personal communications systems and demands on the available frequency spectrum, UWB technology is a good candidate for new generation communications.

Further author information: (Send correspondence to Norman C. Beaulieu)
Norman C. Beaulieu: E-mail: beaulieu@ece.ualberta.ca , Telephone: 1 780 492 5558
Bo Hu: E-mail: bohu@ece.ualberta.ca, Telephone:1 780 492 6469
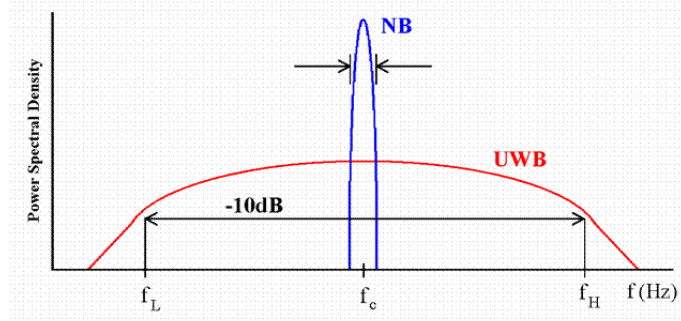
Figure 1. The relationship between the power spectrums of narrowband and UWB systems (from [1]).

There are several motivations that drive the recent investigation on UWB wireless communications. First, fine spatial resolution, low probability of interception and non-interfering signal waveforms are good features that make UWB appealing. The second is the increasing demand for cheap, low power, high bit rate portable wireless devices. UWB systems, with their much wider bandwidths, have much higher capacities and thus can be utilized in future high-capacity wireless systems.

Advantages of UWB communication systems include low power consumption and implementation complexity reductions. The very small power spectral densities of UWB systems ensure only minimal mutual interference between UWB and other communication applications. The fine delay resolution properties make UWB radio a valuable candidate for communications in dense multipath environments and the ultra-wide bandwidth makes the communication robust with respect to multipath fading. The high ratio of the transmitted signal bandwidth to the information signal bandwidth makes UWB technology attractive for multiple access applications. It is for the same reason that spread spectrum techniques are employed to provide multiple access for many users to share an available bandwidth. The application of a time-hopping (TH) sequence in UWB systems to eliminate catastrophic collisions was part of the original proposal for UWB multiple access communication systems [2]. Several modulation techniques have been proposed for UWB signals such as pulse position modulation (PPM) and a variety of pulse amplitude modulations (PAM's) including binary phase-shift keying (BPSK) and on-off keying (OOK) [3].

In this paper, we first introduce UWB system models in general and describe the error rate analysis models used in our work in detail. The expressions for the bit error rate (BER) are then derived for different time-hopping UWB systems based on exact analysis of the multiple access interference. The validity of our analysis is confirmed by simulation and some useful results are provided through numerical examples. Finally, some conclusions are drawn from this study.

2. UWB SYSTEM MODEL

2.1. Time-hopping UWB systems

As mentioned, a TH sequence was incorporated in UWB systems in order to eliminate catastrophic collisions. Time-hopping combined with pulse position modulation (TH-PPM) was originally proposed for UWB communication systems [2]. A typical TH-PPM UWB signal can be described mathematically as follows [4]

$$s\left(t\right) = \sum_{j=-\infty}^{\infty} p\left(t - jT_f - c_j T_c - \delta d_{\lfloor j/N_s \rfloor}^{(k)}\right). \tag{1}$$

Subsequently, time-hopping with binary phase shift keying (TH-BPSK) was proposed; a TH-BPSK UWB signal is written as [5]

$$s_{BPSK}\left(t\right) = \sum_{j=-\infty}^{+\infty} d_{\lfloor j/N_s \rfloor} p\left(t - jT_f - c_j T_c\right) \tag{2}$$
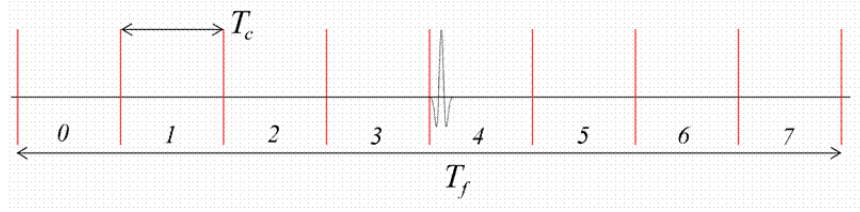
Figure 2. The pulse train structure with TH sequence (from [1]).
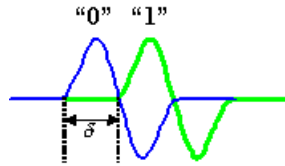
Figure 3. A PPM modulation scheme.

where t is time, $s(t)$ (or $s_{BPSK}(t)$) is the transmitted signal, and $p(t)$ is the signal pulse with pulse width T_p. The structure of time-hopping UWB systems is described as follows [4]:

- *Uniform Pulse Train Spacing:* A uniform pulse train of the form $\sum_{j=-\infty}^{+\infty} p(t - jT_f)$ consists of monocycle pulses spaced T_f seconds apart in time. The *frame time* T_f typically may be a hundred to a thousand times the monocycle width T_p, resulting in a signal with a very low duty cycle.

- *Pseudorandom TH:* Multiple access signals composed of uniformly spaced pulses are vulnerable to occasional catastrophic collisions in which a large number of pulses from different signals are received simultaneously. To eliminate catastrophic collisions in multiple access applications, a distinct pulse-shift pattern $\{c_j\}$ called a *TH sequence* is introduced. T_c is the hop width and satisfies $c_j T_c \leq T_f$. The TH sequence therefore provides an additional time shift to each pulse in the pulse train. In each frame time, the pulse is pseudo-randomly positioned in time with a TH sequence as shown in Fig.2.

- *Modulation Schemes:* The sequence $\{d_j\}$ is a transmitted data sequence. For TH-PPM systems, the data sequence $\{d_j\}_{j=-\infty}^{+\infty}$ is a binary (0 or 1) information stream. In this modulation method, no additional time shift is modulated on the pulse $p(t)$ when the data symbol is 0, but a time shift of δ is added to the pulse when the symbol is 1, shown in Fig. 3. In TH-BPSK systems, $\{d_j\}_{j=-\infty}^{+\infty} \in \{1, -1\}$.

- *Repetition Structure:* From (1) and (2), we note that the modulating data symbol changes only every N_s frames. Assuming that a new data symbol begins with pulse index $j = 0$, the index of the data symbol modulating pulse j is $\lfloor j/Ns \rfloor$. Fig. 4 shows this repetition structure. As we can see, the bit duration $T_b = N_s T_f$. The scheme can also be looked as using a repetition code with the code length of N_s.
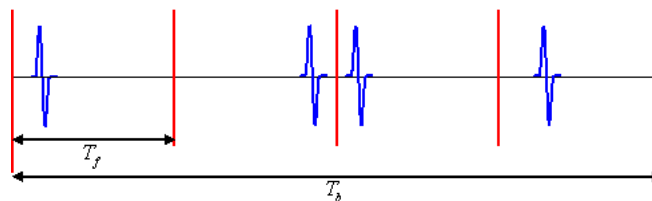
Figure 4. The repetition structure of an information bit.

2.2. Direct sequence UWB systems

It is well-known that direct sequence (DS) spread spectrum (SS) has the ability to combat interference, increase system capacity and improve quality of service. DS-SS has been widely adopted in code division multiple access (CDMA) systems. Although the time-hopping spread spectrum technique was the original method proposed for multiple access UWB communication systems, UWB communication systems using the DS-SS technique have also attracted much interest because of the good features of DS-SS. Similar to conventional DS-CDMA systems, a DS-BPSK UWB system has the mathematical form [6]

$$s_{DS}(t) = \sum_{j=-\infty}^{\infty} \sum_{n=0}^{N_c-1} d_j c_n p(t - jT_f - nT_c) \tag{3}$$

where c_n represents the spreading sequence, T_c is the chip width and N_c is the number of chips per symbol.

3. TH-UWB ERROR RATE ANALYSIS MODEL

Several system models have been introduced in the previous section. Considering time-hopping UWB was the original proposal, we first focus our work on the multiple access interference analysis of TH-UWB. Some studies on TH-UWB systems have been done by other researchers, including the multiple access performance analysis of TH-PPM systems [4] and TH-BPSK systems [5]. Additionally, a performance comparison of TH-PPM and TH-BPSK was described in [7]. However, these studies were conducted based on using a Gaussian approximation for the interference term. It has been shown that the Gaussian approximation may significantly underestimate the BER of TH-PPM systems [8], [9], rendering these results less useful. Our purpose is to provide an analytical method for analyzing the multiple access interference (MAI) of UWB systems and then to evaluate the bit error rate performances of different UWB modulation schemes in the general case using this method. In this paper, we derive exact BER expressions for TH-PPM and TH-BPSK UWB systems in an additive white Gaussian noise (AWGN) environment based on a characteristic function (CF) technique [10], [11]. The AWGN channel model is important in its own right for some UWB applications [4], [12] and is a necessary intermediate step for future work examining UWB on more complex fading channel models.

The asynchronous TH-PPM and TH-BPSK UWB systems are described in [13]; our notation and terminology here are consistent with this paper. A multiple access TH-PPM UWB signal has the form

$$s^{(k)}(t, i) = \sqrt{\frac{E_b}{N_s}} \sum_{j=iN_s}^{(i+1)N_s-1} p\left(t - jT_f - c_j^{(k)}T_c - d_i^{(k)}\delta\right) \tag{4}$$

and a TH-BPSK signal is given by

$$s_{BPSK}^{(k)}(t, i) = \sqrt{\frac{E_b}{N_s}} \sum_{j=iN_s}^{(i+1)N_s-1} d_i^{(k)} p\left(t - jT_f - c_j^{(k)}T_c\right) \tag{5}$$

where $s^{(k)}(t, i)$ is the kth user's signal conveying the ith data bit, E_b is the bit energy common to all signals and $\sqrt{\frac{E_b}{N_s}}$ is a normalization factor. The signal pulse $p(t)$ is normalized so that $\int_{-\infty}^{+\infty} p^2(t)dt = 1$. The sequence $\{c_j^{(k)}\}$ represents the TH code for the kth source and it is pseudorandom with each element taking an integer in the range $0 \le c_j^{(k)} < N_h$, where N_h is the number of hops.

We assume N_u users are transmitting asynchronously on an AWGN channel; the received signal is

$$r(t) = \sum_{k=1}^{N_u} A_k s^{(k)}(t - \tau_k) + n(t) \tag{6}$$

where $n(t)$ is the additive noise with two-sided power spectral density $\frac{N_0}{2}$, $\{A_k\}_{k=1}^{N_u}$ and $\{\tau_k\}_{k=1}^{N_u}$ represents the channel attenuation and time shifts for all transmitted signals, respectively. Consider $s^{(1)}(t)$ to be the desired

signal and $d_0^{(1)}$ to be the transmitted data bit. Without loss of generality, we will further assume $c_j^{(1)} = 0$, for all j [12]. Then $\left\{ s^{(k)} \right\}_{k=2}^{N_u}$ are interference signals. Assuming perfect synchronization with the reference signal $s^{(1)}(t)$, the decision statistic of the single-user correlation receiver is obtained as

$$r = \sum_{j=0}^{N_s-1} \int_{jT_f}^{(j+1)T_f} r(t)v(t - \tau_1 - jT_f)dt \tag{7}$$

where $v(t)$ is the correlation template waveform.

In UWB systems, the choice of the pulse shape will directly affect the bit error rate performance in general. Unlike conventional narrowband communication systems, it is desirable for UWB signals to spread the energy as widely in frequency as possible to minimize the power spectral density and hence the potential for interference to other user systems. A variety of pulse shapes have been proposed for UWB impulse radio systems, which are designed to approach an ideal transmission power spectrum and to avoid having a DC component. In this paper, we restrict our analysis of time-hopping systems to the 2nd-order Gaussian monocycle, given by

$$p\left(t\right) = \left[1 - 4\pi \left(\frac{t}{\tau_p} \right)^2 \right] \exp \left[-2\pi \left(\frac{t}{\tau_p} \right)^2 \right]. \tag{8}$$

Our analytical method, however, can be applied to UWB systems using arbitrary pulse shapes.

4. ANALYSIS OF TH-PPM SYSTEM

For TH-PPM systems, the information bit $d_j^{(k)}$ is assumed to take value 0 or 1 with equal probabilities. In this modulation scheme, the correlator template waveform $v(t)$ has the form [4]

$$v(t) = p(t) - p(t - \delta). \tag{9}$$

Define the correlation of the template $v(t)$ with a time-shifted pulse $p(t)$ as

$$\begin{aligned} \bar{R}(x) &= \int_{-\infty}^{\infty} p(t - x)v(t)dt \\ &= R\left(x\right) - R\left(x - \delta\right) \end{aligned} \tag{10}$$

where $R(x)$ is the autocorrelation of the pulse $p(t)$.

Substituting (6) into (7) yields

$$r = S + I + n \tag{11}$$

where n is a Gaussian random variable (RV) with zero mean and variance $\sigma_n^2 = N_0 N_s \bar{R}(0)$, $S = \pm A_1 \sqrt{E_b N_s} \bar{R}(0)$ is the signal component depending on user 1's useful signal bit $d_0^{(1)}$, and I is the total MAI due to all $N_u - 1$ interfering signals, given by

$$I = \sum_{k=2}^{N_u} \sum_{j=0}^{N_s-1} \int_{jT_f}^{(j+1)T_f} A_k s^{(k)}(t - \tau_k)v\left(t - \tau_1 - jT_f\right)dt. \tag{12}$$

The difference of time shifts for user asynchronism can be modeled as [4, eqn. (55)]

$$\tau_k - \tau_1 = j_k T_f + \alpha_k, \quad -T_f/2 \leq \alpha_k < T_f/2 \tag{13}$$

where j_k is the value of the time difference $\tau_k - \tau_1$ rounded to the nearest frame time, and α_k is uniformly distributed on $[-T_f/2, T_f/2)$. Based on the assumption [4, eqn. (57)], which is rewritten as

$$N_h T_c < T_f/2 - 2T_p \tag{14}$$

where T_p is the pulse width as mentioned, we note that only one pulse from each interfering user in each frame contributes to the interference term. Therefore, (12) can be rewritten in the form [4, eqn. (76)]

$$I = \sqrt{\frac{E_b}{N_s}} \sum_{k=2}^{N_u} \sum_{j=0}^{N_s-1} \int_{-\infty}^{\infty} A_k p \left(x - \alpha_k - c_j^{(k)} T_c - d_{\lfloor (j+j_k)/N_s \rfloor}^{(k)} \delta \right) v(x) dx. \tag{15}$$

Considering that the interfering signal $d_{\lfloor (j+j_k)/N_s \rfloor}^{(k)}$ may change sign during the transmission time of $d_0^{(1)}$, we rewrite (15) as

$$I = \sqrt{\frac{E_b}{N_s}} \sum_{k=2}^{N_u} A_k \left[\sum_{j=0}^{\gamma_k-1} \bar{R} \left(\bar{\Theta}_{0,j}^{(k)} \right) + \sum_{j=\gamma_k}^{N_s-1} \bar{R} \left(\bar{\Theta}_{1,j}^{(k)} \right) \right] \tag{16}$$

where

$$\bar{\Theta}_{0,j}^{(k)} = \alpha_k + c_j^{(k)} T_c + d_0^{(k)} \delta \tag{17}$$

and

$$\bar{\Theta}_{1,j}^{(k)} = \alpha_k + c_j^{(k)} T_c + d_{-1}^{(k)} \delta \tag{18}$$

and where $d_0^{(k)}$ and $d_{-1}^{(k)}$ represent the two adjacent bits of the kth signal that overlap with the transmission time of $d_0^{(1)}$. According to the definition of j_k in (13), γ_k is uniform over $[0, N_s - 1]$.

Similar to the analytical procedure provided in [13], we can calculate the CF of the interference I by averaging the conditional CF of MAI step by step. First, we express the probability density function (pdf) of $\bar{\Theta}_{0,j}^{(k)}$ conditioned on $d_0^{(k)}$ for a given α_k as

$$f_{\bar{\Theta}_0|d,\alpha} \left(\bar{\theta} | d_0^{(k)} = d, \alpha_k = \alpha \right) = \frac{1}{N_h} \sum_{h=0}^{N_h-1} \delta_D(\bar{\theta} - hT_c - \delta d - \alpha) \tag{19}$$

where $\delta_D(\cdot)$ is the Dirac delta function. The CF of $\bar{R}(\bar{\Theta}_{0,j}^{(k)})$ conditioned on $d_0^{(k)}$ and α_k can be written as

$$\Phi_{\bar{R}_0|d,\alpha}(\omega) = E \left[e^{j\omega \bar{R}_0} | d_0^{(k)} = d, \alpha_k = \alpha \right]$$

$$= \frac{1}{N_h} \sum_{h=0}^{N_h-1} e^{j\omega \bar{R}(\alpha + hT_c + \delta d)} \tag{20}$$

where $E[\cdot]$ denotes expectation. In order to simplify the notation, we further define $X^{(k)} = \sum_{j=0}^{\gamma_k-1} \bar{R} \left(\bar{\Theta}_{0,j}^{(k)} \right)$ and $Y^{(k)} = \sum_{j=\gamma_k}^{N_c-1} \bar{R} \left(\bar{\Theta}_{1,j}^{(k)} \right)$; then

$$I = \sqrt{\frac{E_b}{N_s}} \sum_{k=2}^{N_u} A_k I^{(k)}$$

$$= \sqrt{\frac{E_b}{N_s}} \sum_{k=2}^{N_u} A_k \left(X^{(k)} + Y^{(k)} \right). \tag{21}$$

The conditional CF of $X^{(k)}$ is obtained as

$$\Phi_{X^{(k)}|d,\alpha,\gamma}(\omega) = E \left[e^{j\omega \sum_{j=0}^{\gamma_s-1} \bar{R} \left(\bar{\Theta}_{0,j}^{(k)} \right)} | d_0^{(k)} = d, \alpha_k = \alpha, \gamma_k = \gamma \right]$$

$$= \left(\frac{1}{N_h} \sum_{h=0}^{N_h-1} e^{j\omega \bar{R}(\alpha + hT_c + \delta d)} \right)^{\gamma} \tag{22}$$

where the second equality follows from the fact that $\bar{R}(\bar{\Theta}_{0,j}^{(k)})$, $j = 0, ..., \gamma_s - 1$, are independent when conditioned on $d_0^{(k)}$ and α_k. Therefore, the CF of $X^{(k)}$ conditioned on α_k and γ_k can be obtained as

$$\Phi_{X^{(k)}|\alpha,\gamma}(\omega) = \Phi_{X^{(k)}|0,\alpha,\gamma}(\omega)\Pr(d = 0) + \Phi_{X^{(k)}|1,\alpha,\gamma}(\omega)\Pr(d = 1)$$

$$= \frac{1}{2N_h^\gamma}\left[\left(\sum_{h=0}^{N_h-1}e^{j\omega\bar{R}(\alpha+hT_c)}\right)^\gamma + \left(\sum_{h=0}^{N_h-1}e^{j\omega\bar{R}(\alpha+hT_c+\delta)}\right)^\gamma\right]. \tag{23}$$

Similarly, the CF of $Y^{(k)}$ conditioned on α_k and γ_k can be obtained as

$$\Phi_{Y^{(k)}|\alpha,\gamma}(\omega) = \frac{1}{2N_h^{N_s-\gamma}}\left[\left(\sum_{h=0}^{N_h-1}e^{j\omega\bar{R}(\alpha+hT_c)}\right)^{N_s-\gamma} + \left(\sum_{h=0}^{N_h-1}e^{j\omega\bar{R}(\alpha+hT_c+\delta)}\right)^{N_s-\gamma}\right]. \tag{24}$$

It can be shown that the RV's $X^{(k)}$ and $Y^{(k)}$ are independent for given k, which results from the independence of the data bits (d_0 and d_{-1}), and the independence of the chip sequences (with distinct chip index, j). Then, the CF of $I^{(k)}$ conditioned on α_k and γ_k is given by

$$\Phi_{I^{(k)}|\alpha,\gamma}(\omega) = \Phi_{X^{(k)}|\alpha,\gamma}(\omega)\Phi_{Y^{(k)}|\alpha,\gamma}(\omega). \tag{25}$$

The CF of $I^{(k)}$ conditioned on α_k can be obtained based on the uniform distribution of γ_k as

$$\Phi_{I^{(k)}|\alpha}(\omega) = \frac{1}{N_s}\sum_{i=0}^{N_s-1}\left[\Phi_{X^{(k)}|\alpha,i}(\omega)\Phi_{Y^{(k)}|\alpha,i}(\omega)\right]. \tag{26}$$

Averaging out α_k, we obtain the CF of the kth interferer as

$$\Phi_{I^{(k)}}(\omega) = \frac{1}{T_f}\int_{-T_f/2}^{T_f/2}\Phi_{I^{(k)}|\alpha}(\omega)d\alpha. \tag{27}$$

Owing to the independence of the interfering components, the CF of the total interference is [13]

$$\Phi_I(\omega) = \prod_{k=2}^{N_u}\Phi_{I^{(k)}}\left(A_k\sqrt{\frac{E_b}{N_s}}\omega\right). \tag{28}$$

5. ANALYSIS OF TH-BPSK SYSTEM

The template waveform used in TH-BPSK systems is the pulse $p(t)$ [5], which is different from the template waveform $v(t)$ used in TH-PPM systems. The decision statistic r_{BPSK} is then calculated using this correlator template as

$$r_{BPSK} = S_{BPSK} + I_{BPSK} + n_{BPSK} \tag{29}$$

where n_{BPSK} is a Gaussian noise with zero mean and variance $\sigma_{n_{BPSK}}^2 = \frac{N_0N_s}{2}R(0)$, $S_{BPSK} = A_1\sqrt{E_bN_s}d_0^{(1)}R(0)$ depends on user 1's useful signal bit $d_0^{(1)}$, and I_{BPSK} is the total MAI in the TH-BPSK UWB system, given by

$$I_{BPSK} = \sqrt{\frac{E_b}{N_s}}\sum_{k=2}^{N_u}A_k\left[\sum_{j=0}^{\gamma_k-1}d_0^{(k)}R\left(\Theta_j^{(k)}\right) + \sum_{j=\gamma_k}^{N_s-1}d_{-1}^{(k)}R\left(\Theta_j^{(k)}\right)\right] \tag{30}$$

where $\Theta_j^{(k)} = \alpha_k + c_j^{(k)}T_c$. Similar to (20), the CF of $R(\Theta_j^{(k)})$ conditioned on α_k can be written as

$$\Phi_{R|\alpha}(\omega) = E\left[e^{j\omega R}|\alpha_k = \alpha\right] = \frac{1}{N_h}\sum_{h=0}^{N_h-1}e^{j\omega R(\alpha+hT_c)}. \tag{31}$$

Define $X_{BPSK}^{(k)} = \sum_{j=0}^{\gamma_k-1} d_0^{(k)} R\left(\Theta_j^{(k)}\right)$ and $Y_{BPSK}^{(k)} = \sum_{j=\gamma_k}^{N_s-1} d_{-1}^{(k)} R\left(\Theta_j^{(k)}\right)$, then

$$
\begin{aligned}
I_{BPSK} &= \sqrt{\frac{E_b}{N_s}} \sum_{k=2}^{N_u} A_k I_{BPSK}^{(k)} \\
&= \sqrt{\frac{E_b}{N_s}} \sum_{k=2}^{N_u} A_k \left[X_{BPSK}^{(k)} + Y_{BPSK}^{(k)} \right].
\end{aligned}
\tag{32}
$$

The CF of $X_{BPSK}^{(k)}$ conditioned on α_k and γ_k is obtained as

$$
\Phi_{X^{(k)}|\alpha,\gamma} = \frac{1}{2N_h{}^\gamma} \left[\left(\sum_{h=0}^{N_h-1} e^{j\omega R(\alpha+hT_c)} \right)^\gamma + \left(\sum_{h=0}^{N_h-1} e^{-j\omega R(\alpha+hT_c)} \right)^\gamma \right].
\tag{33}
$$

and the conditional CF of $Y_{BPSK}^{(k)}$ can be obtained similarly.

Based on the conditional CF's of $X_{BPSK}^{(k)}$ and $Y_{BPSK}^{(k)}$, the CF of $I_{BPSK}^{(k)}$ conditioned on α_k and γ_k is given by

$$
\Phi_{I_{BPSK}^{(k)}|\alpha,\gamma}(\omega) = \Phi_{X^{(k)}|\alpha,\gamma}(\omega)\Phi_{Y^{(k)}|\alpha,\gamma}(\omega).
\tag{34}
$$

Using the uniform distributions of $\{\alpha_k\}_{k=2}^{N_u}$ and $\{\gamma_k\}_{k=2}^{N_u}$, we can obtain the CF of $I_{BPSK}^{(k)}$ as

$$
\Phi_{I_{BPSK}^{(k)}}(\omega) = \frac{1}{T_f N_s} \int_{-T_f/2}^{T_f/2} \sum_{i=0}^{N_s-1} \Phi_{X^{(k)}|\alpha,i}(\omega)\Phi_{Y^{(k)}|\alpha,i}(\omega) d\alpha.
\tag{35}
$$

Finally, the CF of the total interference in the TH-BPSK system is given by

$$
\Phi_{I_{BPSK}}(\omega) = \prod_{k=2}^{N_u} \Phi_{I_{BPSK}^{(k)}} \left(A_k \sqrt{\frac{E_b}{N_s}} \omega \right).
\tag{36}
$$

6. BIT ERROR PROBABILITY

Based on the previous analysis, we will determine expressions for the bit error probabilities of the TH-PPM and TH-BPSK UWB systems in this secion. The decision rule for the TH-PPM system is [4]

$$
\begin{aligned}
r > 0 &\Rightarrow \text{``0''} \\
r \le 0 &\Rightarrow \text{``1''}
\end{aligned}
$$

and the decision rule for the TH-BPSK UWB systems is [5]

$$
\begin{aligned}
r > 0 &\Rightarrow \text{``1''} \\
r \le 0 &\Rightarrow \text{``-1''}.
\end{aligned}
$$

Owing to the symmetry of the MAI and the noise , which has been explained in [4], the average probability of error for the TH-PPM system is given by

$$
\begin{aligned}
P_e &= \Pr(r \le 0 \mid d = 0) \\
&= \Pr(A_1\sqrt{E_b N_s}\bar{R}(0) + I + n \le 0)
\end{aligned}
\tag{37}
$$

and the BER for the TH-BPSK systems is

$$
\begin{aligned}
P_e &= \Pr(r \le 0 \mid d = 1) \\
&= \Pr(A_1\sqrt{E_b N_s}R(0) + I_{BPSK} + n_{BPSK} \le 0).
\end{aligned}
\tag{38}
$$

Define $\Lambda = I + n$. Based on the independence of the MAI and the background noise, the CF of Λ can be expressed as the product of the CF of the interfering signals I and the CF of the Gaussian noise as

$$\Phi_\Lambda(\omega) = \Phi_I(\omega)\Phi_n(\omega) \tag{39}$$

where $\Phi_n(\omega) = e^{\frac{-\sigma_n^2 \omega^2}{2}}$ is the CF for the noise term n and $\Phi_I(\omega)$ is the CF of MAI in the TH-PPM or TH-BPSK system.

As known, the cumulative density function (cdf) of Λ can be expressed as the inverse transform of the characteristic function of Λ as at [14, eqn. (3-23)], given by

$$F_\Lambda(\lambda) = \frac{1}{2} + \frac{1}{\pi}\int_0^\infty \frac{\sin(\lambda\omega)}{\omega}\Phi_\Lambda(\omega)d\omega. \tag{40}$$

Then, the average probability of error for the desired user in the TH-PPM system is given by

$$\begin{aligned} P_e &= 1 - F_\Lambda\left(A_1\sqrt{E_b N_s}\bar{R}(0)\right) \\ &= \frac{1}{2} - \frac{1}{\pi}\int_0^\infty \frac{\sin(A_1\sqrt{E_b N_s}\bar{R}(0)\omega)}{\omega}\Phi_I(\omega)\exp\left(\frac{-\sigma_n^2\omega^2}{2}\right)d\omega \end{aligned} \tag{41}$$

and the BER for the TH-BPSK UWB systems is obtained as

$$\begin{aligned} P_{e_{BPSK}} &= 1 - F_\Lambda\left(A_1\sqrt{E_b N_s}R(0)\right) \\ &= \frac{1}{2} - \frac{1}{\pi}\int_0^\infty \frac{\sin(A_1\sqrt{E_b N_s}R(0)\omega)}{\omega}\Phi_{I_{BPSK}}(\omega)\exp\left(\frac{-\sigma_{n_{BPSK}}^2\omega^2}{2}\right)d\omega. \end{aligned} \tag{42}$$

7. NUMERICAL RESULTS AND COMPARISONS

In this section, some numerial examples will be presented to assess our analytical expressions and performance evaluation using these expressions will be described. It is seen from (41) and (27), or (42) and (35) that a double-integral calculation is required for computing the BER of TH-UWB systems. This double integration is performed numerically, but is not problematic. Our trials indicated that simple numerical integration techniques can be used to obtain the BER to any reasonable desired accuracy. Additionally, Monte Carlo simulation was used to validate our analytical derivations. We simulated the decision statistics including eqns. (11) and (29) using Matlab. Uniformly distributed RV's and Gaussian distributed RV's used in the simulation of the decision statistics were generated using random number generators provided by Matlab.

We first compare the exact BER's of TH-UWB systems with results obtained from simulations and the Gaussian approximation. In the Gaussian approximation, the expression for signal-to-interference-plus-noise ratio (SINR) follows [4, eqn. (44)], given by

$$\text{SINR}(N_u) = \frac{S^2}{\sigma_n^2 + N_s\sigma_a^2\sum_{k=2}^{N_u} A_k^2} \tag{43}$$

where σ_n^2 is the variance of the noise component and the parameter σ_a^2 is defined as [4, eqn. (79)]

$$\sigma_a^2 = \frac{1}{T_f}\int_{-\infty}^\infty \left[\int_{-\infty}^\infty p(x-s)v(x)dx\right]^2 ds. \tag{44}$$

In addition, the performance of TH-PPM and TH-BPSK systems will be evaluated for different pulse parameters. Some comparisons between two different UWB modulation systems in terms of BER are presented as well. Most of the numerical results presented in this paper are based on analysis using the 2nd-order Gaussian monocycle. Results for the 4th-order monocycle are also provided here to show the effects of changing the pulse shape. The parameters of the example UWB systems are listed in Table I and follow [4] and [12] except T_f, which is chosen

Table 1. Parameters of the Example TH-PPM and TH-BPSK systems

Parameter	Notation	2nd and 4th order monocycles
Time Normalization Factor	τ_p	0.2877 ns
Impulse Width	T_p	$\approx$ 0.7 ns
Frame Width	T_f	50 ns
PPM Delay	δ	0.15 ns
Chip Width	T_c	0.9 ns
Number of Users	N_u	8
Number of Chips per Frame	N_h	8
Repetition Code Length	N_s	2, 4, 16, 50 or 100
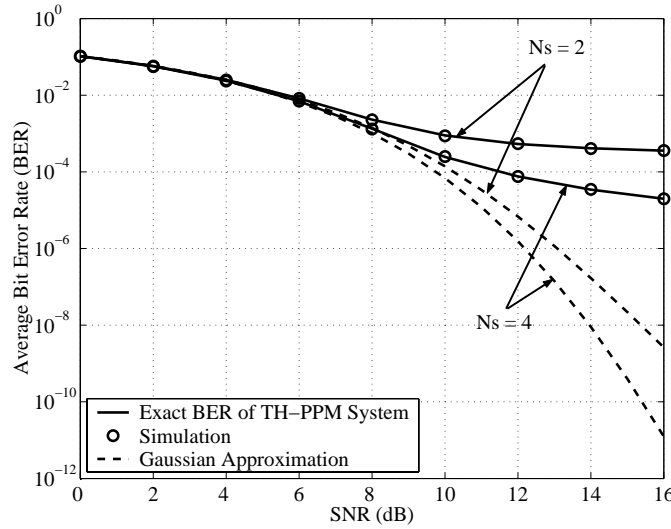
Figure 5. Average BER of the TH-PPM UWB system versus SNR for a repetition code with $N_s = 2$ and $N_s = 4$ assuming 7 asynchronous interferers.

to be 50 ns to satisfy (14). Actually, there can be more than one pulse from each interfering user in each frame contributing to the interference term if condition (14) is removed. In this case, the new expression for the MAI complicates the analysis of TH-UWB systems. However, the CF method presented in this paper can circumvent this difficulty and can still be applied for analyzing interference in TH-UWB systems as shown in [15].

Fig. 5 shows the accurate BER's of the TH-PPM system computed using the CF method derived in Section 6 , as well as the BER's obtained from the Gaussian approximation and simulation. In our work, signal-to-noise power ratio (SNR) is defined as $\frac{E_b}{N_0}$. As seen, the theoretical results and the simulation results are in excellent agreement. Comparing the BER's obtained from the exact analysis with the BER's obtained from the Gaussian approximation, we can see that the Gaussian approximation is in good agreement with the exact analysis only for small SNR values and the Gaussian approximation fails to predict the error rate floor of the TH-PPM UWB system (caused by the multiple access interference) for large SNR values. Fig. 5 also indicates that the BER performance improves when the longer repetition code is used, as expected. Observe that the amount of the improvement can be less or more than the improvement predicted by the Gaussian approximation. For example, when the SNR = 9 dB, the amount of the improvement due to the longer repetition code predicted by the Gaussian approximation is less than the actual improvement; when the SNR = 16 dB, the amount of improvement predicted by the Gaussian approximation is more than the actual improvement. Thus, the Gaussian approximation is not a reliable tool for predicting the bit error rate of TH-UWB systems.
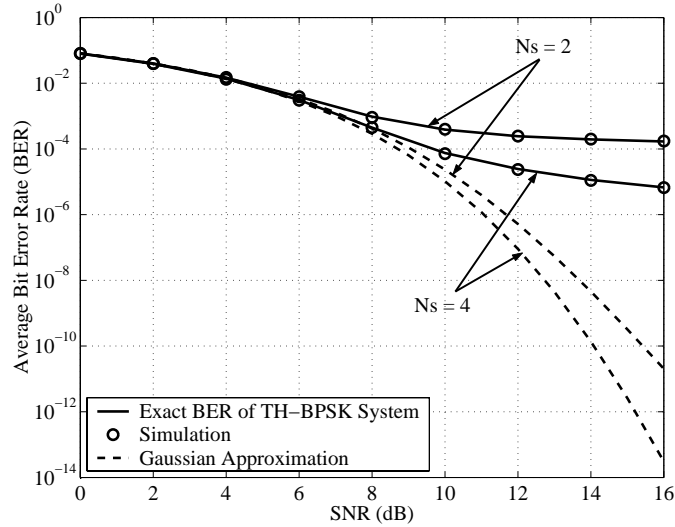
Figure 6. Average BER of the TH-BPSK UWB system versus SNR for a repetition code with $N_s = 2$ and $N_s = 4$ assuming 7 asynchronous interferers.

Fig. 6 shows the BER results for the TH-BPSK system obtained from the exact analysis, the Gaussian approximation and simulation as well. From our numerical examples, we observe that the BER estimates based on the Gaussian approximation also underestimate the accurate BER of the TH-BPSK system for medium and large SNR values as in the TH-PPM system. Similar to the results seen in Fig. 5, Fig. 6 shows that the Gaussian approximation fails to predict the error rate floor caused by the interference and that the Gaussian approximation can underestimate or overestimate the improvement obtained by using a longer repetition code.

In order to assess the accuracy of the Gaussian approximation at high values of N_s, we also provide numerical results for TH-UWB systems with $N_s = 16$, 50 and 100 shown in Figs. 7 and 8 taken from [13]. Fig. 7 shows the accurate BER results for the TH-PPM system and the BER obtained from the Gaussian approximation for $N_s = 16$, 50 and 100. It is seen that the Gaussian approximation improves for the longer repetition codes in the sense that it is accurate for a wider range of values of SNR. For example, while the Gaussian approximation is highly accurate only for SNR ≤ 6 dB when $N_s = 2$, it is highly accurate for SNR ≤ 10 dB when $N_s = 100$. Nonetheless, the Gaussian approximation still underestimates the BER's of TH-PPM systems at larger values of N_s. Similar behavior is also observed for the BER's of the TH-BPSK system with different values of N_s as indicated in Fig. 8. In the Gaussian approximation, the BER's are obtained by modeling the total MAI as a Gaussian distributed RV. In fact, we can show that the MAI is not Gaussian distributed. For small values of SNR, the background Gaussian noise n is dominant in the term $\Lambda = I + n$, and then Λ can be approximated as a Gaussian distributed RV. Therefore, the Gaussian approximation can provide good BER estimates for small SNR. On the other hand, when SNR is large, the interference I is dominant in the term Λ, and Λ cannot be approximated as a Gaussian distributed RV. Thus, the Gaussian approximation fails to predict the BER's accurately for large values of SNR as indicated in Figs. 5-8.

As known, the pulse plays an important role in determining the performance of the TH-UWB systems. In Fig. 9, the impact of the pulse shape on the average BER's of the TH-PPM UWB system for different Gaussian monocycles and different pulse widths is examined. The dotted lines with triangle markers denote the BER's of the TH-PPM system using the 2nd-order Gaussian monocycle with original parameters as given in Table I. The dotted lines with star markers denote the BER's of the TH-PPM system for the 2nd-order monocycle with larger τ_p, corresponding to a larger pulse width. We observe that the performance using the 2nd-order monocycle with smaller τ_p is better than the performance using the same order monocycle with larger τ_p, for all SNR values. When τ_p is fixed, the 4th-order Gaussian monocycle outperforms the 2nd-order monocycle as indicated by the solid lines with circle markers. It seems that the higher-order Gaussian monocycle can provide lower multiple
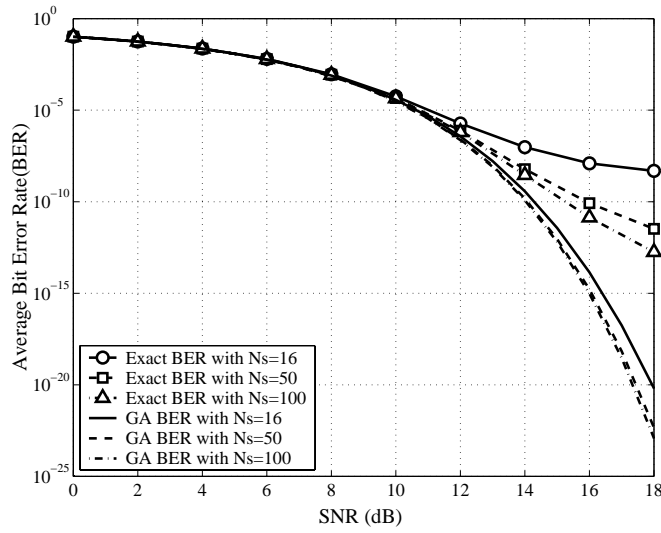
Figure 7. Average BER of the TH-PPM UWB system versus SNR for a repetition code with $N_s = 16$, $N_s = 50$ and $N_s = 100$.
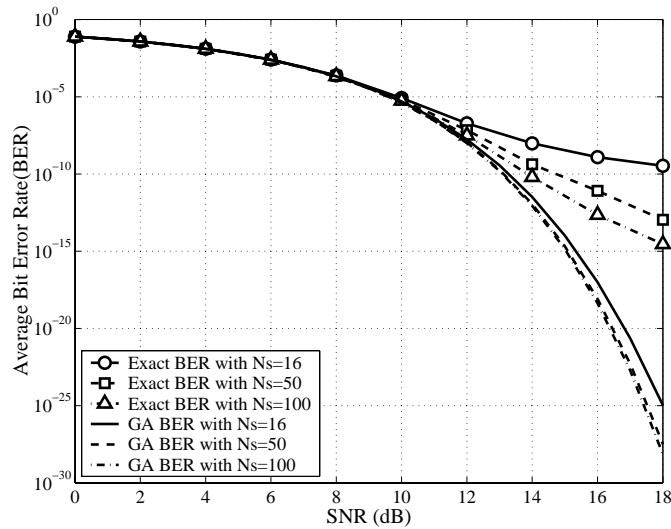
Figure 8. Average BER of the TH-BPSK UWB system versus SNR for a repetition code with $N_s = 16$, $N_s = 50$ and $N_s = 100$.
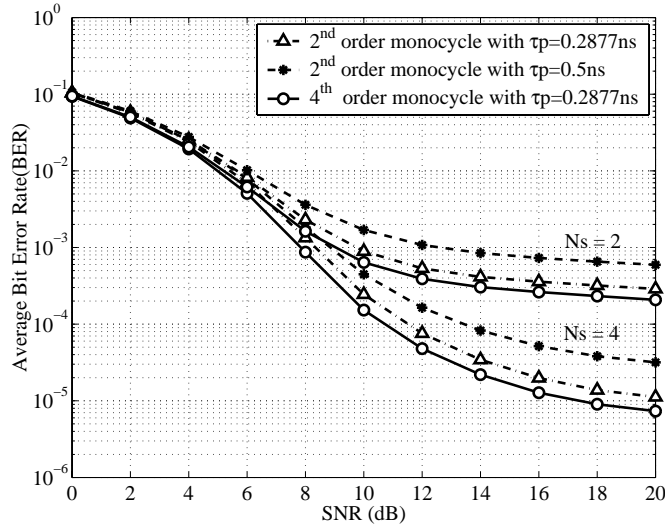
Figure 9. Comparison of the TH-PPM systems using different Gaussian monocycles for a repetition code with $N_s = 2$ and $N_s = 4$ assuming 7 asynchronous interferers.

access bit error rates when the pulse width is fixed, and that the same order monocycle with smaller pulse width provides lower bit error rates. These results can be explained by comparing the autocorrelation functions of the Gaussian monocycles. Actually, our observations are consistent with those reported in [16], obtained from a SNR analysis using a Gaussian approximation.

The performance of the TH-BPSK UWB system for different Gaussian monocycles and pulse widths is plotted in Fig. 10. Unlike the TH-PPM system, when τ_p is fixed, the TH-BPSK system shows almost the same bit error rates for Gaussian monocycles with different orders except for large values of SNR, where the performance of the higher-order Gaussian monocycle is slightly better than the performance of the lower-order Gaussian monocycle with the same t_p. However, Gaussian monocycles of the same order, but with smaller pulse widths also provide lower bit error rates as in the TH-PPM system. This behaviour results directly from the features of the autocorrelation functions of different monocycles.

Fig. 11 shows a performance comparison of the TH-BPSK and TH-PPM UWB systems with the 2nd-order Gaussian monocycle. It is obvious that the TH-BPSK system outperforms the TH-PPM system for all values of SNR. Our observation is consistent with the result in [17], which states that the TH-BPSK system yields better performance than the TH-PPM UWB system. The conclusion in [17] was reached according to analysis based on chip-synchronous systems, which is a simpler case of MAI environments. Here the same conclusion is reached but for chip-asynchronous systems, which are more common in practical applications.

8. CONCLUSION

In this paper, we have derived accurate, analytical expressions for the average probability of bit error of TH-PPM and TH-BPSK UWB systems based on an exact analysis of the multiple access interference. In contrast to the Gaussian appoximation, which substantially overestimates the BER of TH-UWB systems for medium and large SNR values, our analysis provides accurate BER estimates for arbitary SNR values. Compared with other methods used in the performance analysis of UWB systems, our analysis provides a powerful tool for calculating BER's to any desired accuracy with very low complexity.

Unlike some previous results that are limited to the systems using a rectangular pulse [18], our analytical method can be applied to UWB systems using arbitrary pulse shapes. This gives more flexibility for investigating the effects of different pulse shapes on UWB performance. Using the exact analysis, the effects of the order of Gaussian monocycles and the corresponding pulse parameters on the performances of TH-PPM and TH-BPSK
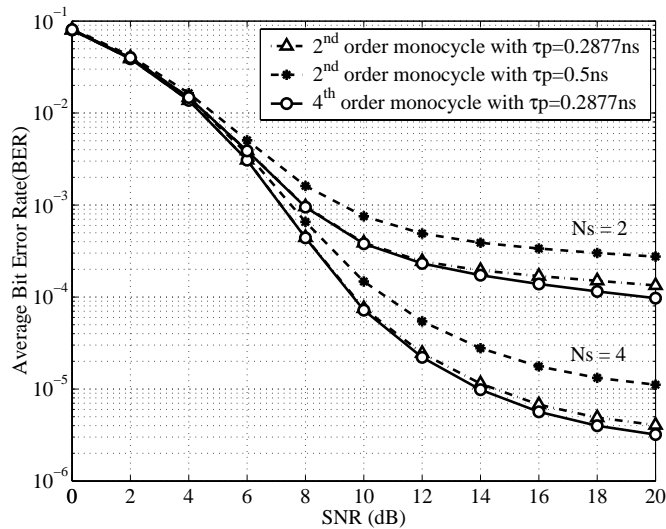
Figure 10. Comparison of the TH-BPSK systems using different Gaussian monocycles for a repetition code with $N_s = 2$ and $N_s = 4$ assuming 7 asynchronous interferers.
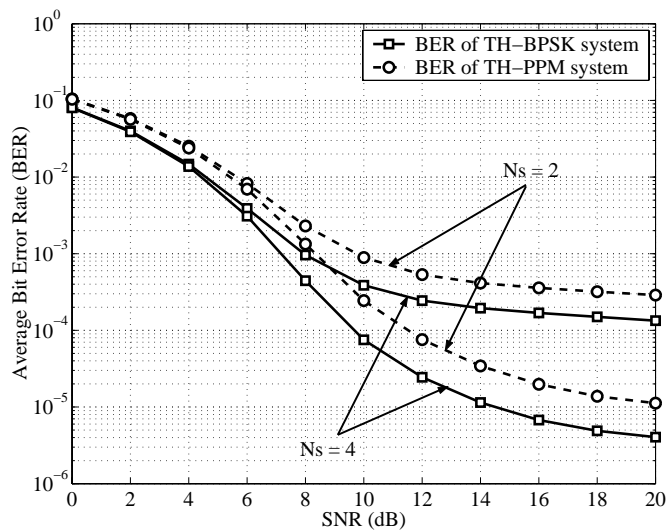
Figure 11. Comparison of the TH-BPSK and TH-PPM systems for a repetition code with $N_s = 2$ and $N_s = 4$ assuming 7 asynchronous interferers.

systems have been briefly examined. Examples indicated that among Gaussian monocycles of the same order those with a smaller pulse width have better multiple access performance. In general, higher-order Gaussian monocycles have better performances than lower-order Gaussian monocycles for a fixed pulse width. Additionally, the comparison of the performances of TH-PPM and TH-BPSK UWB systems, as measured by the average probability of bit error, showed that the TH-BPSK system outperforms the TH-PPM system for all values of SNR. This analytical result confirms the results obtained in past work by other authors using approximate analyses. The comparison, based on the exact analysis, provides important and valuable criteria for choosing appropriate modulation schemes in the design of practical UWB systems.

REFERENCES

1. J. Reed, R. M. Buehrer, and D. S. Ha, *Introduction to UWB: Impulse radio for radar and wireless communications*, Virginia Polytechnic Institute & State University.
2. M. Z. Win and R. A. Scholtz, "Impulse radio: How it works," *IEEE Commun. Lett.* **2**, pp. 51–53, Feb. 1998.
3. M. L. Welborn, "System consideration for ultra-wideband wireless networks," *Proc. IEEE Radio and Wireless Conference*, pp. 5–8, Aug. 2001.
4. M. Z. Win and R. A. Scholtz, "Ultra-wide bandwidth time-hopping spread-spectrum impulse radio for wireless multiple-access communications," *IEEE Trans. Commun.* **48**, pp. 679–691, Apr. 2000.
5. A. Taha and K. M. Chugg, "A theoretical study on the effects of interference on uwb multiple access impulse radio," *Proc. Asilomar Conference on Signals, Systems and Computers*, pp. 728–732, Nov. 2002.
6. N. Boubaker and K. B. Letaief, "Ultra wideband dsss for multiple access communications using antipodal signaling," *Proc. IEEE ICC 2003*, pp. 2197–2201, May 2003.
7. V. S. Somayazulu, "Multiple access performance in uwb systems using time hopping vs. direct sequence spreading," *Proc. WCNC'2002*, pp. 522–525, Mar. 2002.
8. G. Durisi and G. Romano, "On the validity of gaussian approximation to characterize the multiuser capacity of uwb th-ppm," *Proc. IEEE Conf. on Ultra Wideband Systems and Technologies*, May 2002.
9. B. Hu and N. C. Beaulieu, "Exact bit error rate analysis of th-ppm uwb systems in the presence of multiple access interference," *IEEE Commun. Lett.* **7**, pp. 572–574, Dec. 2003.
10. J. Cheng and N. C. Beaulieu, "Accurate ds-cdma bit error probability calculation in rayleigh fading," *IEEE Trans. Wireless Commun.* **1**, pp. 3–15, Jan. 2002.
11. N. C. Beaulieu, "The evaluation of error probabilities for intersymbol and cochannel interference," *IEEE Trans. Commun.* **39**, pp. 1740–1749, Dec. 1991.
12. G. Durisi and S. Benedetto, "Performance evaluation of th-ppm uwb systems in the presence of multiuser interference," *IEEE Commun. Lett.* **7**, pp. 224–226, May 2003.
13. B. Hu and N. C. Beaulieu, "Accurate evaluation of multiple access performance in th-ppm and th-bpsk uwb systems," submitted.
14. A. Papoulis, *The Fourier Integral and its Applications*, McGraw-Hill, New York, 1962.
15. B. Hu and N. C. Beaulieu, "Performance evaluation of time-hopping and direct-sequence uwb systems," in preparation.
16. J. Zhang, T. D. Abhayapala, and R. A. Kennedy, "Performance of ultra-wideband correlator receiver using gaussian monocycles," *Proc. IEEE ICC 2003*, pp. 2192–2196, May 2003.
17. G. Durisi and S. Benedetto, "Performance evaluation and comparison of different modulation schemes for uwb multiaccess systems," *Proc. IEEE ICC 2003*, pp. 2187–2191, May 2003.
18. K. A. Hamdi and X. Gu, "Bit error rate analysis for th-cdma/ppm impulse radio networks," *Proc. WCNC'2003*, Mar. 2003.